PCCP

Accepted Manuscript

ROYAL SOCIETY OF CHEMISTRY

www.rsc.org/pccp

Journal Name

ARTICLE TYPE

Cite this: DOI: 10.1039/xxxxxxxxxx

Adsorption energy of small molecules on core-shell Fe@Au nanoparticles : tuning by shell thickness

Magali Benoit,*[a] Nathalie Tarrat,[a] and Joseph Morillo[a]

Received Date
Accepted Date

DOI: 10.1039/xxxxxxxxxx

www.rsc.org/journalname

The adsorption of several small molecules on different gold surfaces, Au(001), strained Au(001) and Au(001) epitaxied on Fe(001), has been characterized using density functional theory. The surface strain leads to a less energetically favourable adsorption for all studied molecules. Moreover, the presence of the iron substrate induces an additional decrease of the binding energy, for 1 and 2 Au monolayers. For carbon monoxide CO, the structural and energetic variations with the number of Au monolayers deposited on Fe have been analyzed and correlated with the distance between the carbon atom and the gold surface. The effect of the subsurface layer has been evidenced for 1 and 2 monolayers. The other molecules show different quantitative behavior depending on the type of their interaction with the gold surface. However, the iron substrate weakens the interaction, either for the chemisorbed species or for the physisorbed ones. 2 Au monolayers seems like the best compromise to decrease the reactivity of the gold surface towards adsorption while preventing the Fe oxidation.

1 Introduction

Controlling the surface properties of metallic nanoparticles (NP) is one of the current major challenges since these properties determine the way the NPs interact with their environment - a crucial issue for catalysis and biomedical applications.

In catalysis, the surface properties are used in order to promote a specific chemical reaction[1]. The catalytic efficiency of the NP depends on several key factors: the capacity of the NP surface to adsorb the reactants, the activation energy, and the catalyst regeneration efficiency *i.e.* the degree of pollution of the catalytic surface by the reaction products[2]. Indeed, the saturation of the NP surface by the products causes loss of catalytic rate over time. Understanding the factors influencing the surface reactivity of these NPs is unescapable to better control it. It is well known that the presence of sub-coordinated atoms at the surface of NPs (corners and edges of NPs facets, for example), is a key factor for catalysis. Thus, reducing the size of the NP leads to an increase catalytic activity due to the presence of a larger number of these active sites at the NP surface[3,4]. On the other hand, metallic NPs deposited on some oxyde surfaces exhibit enhanced catalytic activity due to a modification of their surface electronic properties[5–8]. In addition, the adsorption energies of reactants and products of a catalytic reaction are different depending on the crystalline facets present at the NP surface.

In the case of biomedical applications, one rather wants that the surface reactivity of a NP is as minimal as possible, while being capable of adsorbing some functional molecules that will be used for drug delivery, for instance. It is also the adsorption energies at some of the NP facets that will determine their grafting and the stability of the nano-conjugates. It is therefore essential to control these adsorption energies, and it would be particularly interesting to even have a way to adjust them.

One possible way to achieve a control of the adsorption of molecules on the surface of a NP is to control its morphology. Indeed, using appropriate growth techniques, it is possible to produce NPs exhibiting specific crystalline facets, on which molecules will adsorb (or not) with different energies[9,10]. Another way to change the adsorption energies of molecules on the surface of NPs consists in deforming the surface. Indeed, studies conducted on the adsorption of small molecules on transition metal surfaces epitaxied on substrates of different natures, showed that the in-plane strain of the metallic surface induced by epitaxy produces a shift of the surface *d*-band states and so a modification of the adsorption energy[11–16]. Finally, it is possible to change the surface reactivity also by modifying the surface electronic structure through the deposition of one or two monolayers of the metal of interest on another metal. In addition to the strain effect due to the epitaxy, the metallic surface properties can be modified by forming a surface alloy or, for non-miscible systems, by an orbital hybridization of the two metals in contact[20–34]. This latter effect is documented under the name of "ligand effect".

In this work, we propose to show that it is possible to tune the adsorption energies of specific molecules on the surface of core-

[a] CEMES-CNRS, 29 rue Jeanne Marvig, 31055 Toulouse Cedex, France; Email: mbenoit@cemes.fr

shell Fe@Au NPs by using both strain and ligand effects. For this, we rely on the properties of facetted core-shell nanoparticles, in which the shell metal component is epitaxied on the core metal component. The lattice mismatch between the core and the shell causes the deformation of the shell surface and thus a change of its properties. Moreover, by varying the shell thickness, we show that additional change of the adsorption energies can be obtained using the ligand effect.

DFT calculations have been carried out on models of the core-shell Fe@Au nanoparticles with well-defined facets obtained by vapor phase deposition. In particular, these NPs display Au(001) planes epitaxied on Fe(001) planes with the following orientation relationship Au(100)[011]//Fe(100)[010][35–37]. Tuning the reactivity of such NPs is particularly important since these nano-objects are susceptible to be used in an organic environment for different biomedical applications such as hyperthermia, targeted drug delivery, imaging or phototherapy[38–40]. The Fe magnetic core is here preserved from oxidation by coating with the bio-compatible Au shell.

The paper is organized as follows. First, the description of the systems used to model the Fe@Au core-shell NPs of different shell thicknesses is given and the simulation details are presented. Then, the results obtained for the adsorption of CO on different systems, from pure Au(001) to Au(001)/Fe(001) with several shell thicknesses, are presented and analyzed in details. Then, the effects of strain and ligand are studied for different molecules, H, H_2O, HCOOH and CH_3S^-. At the end of the paper, these results are discussed.

2 Simulation details

The purpose of this work is to study the surface properties of Fe@Au nanoparticles which exhibit mainly Au(001) facets. Due to their particular morphology, the Fe@Au nanoparticles are characterized by the presence of almost only Fe(001)/Au(001) interfaces between the core and the shell. Moreover, their surface exhibits almost exclusively Au(001) facets as well as very small Au(111) facets[35]. Therefore, in a first approximation, we considered that model systems made of infinite slabs of Au(001) deposited on Fe(001) in the Au(100)[011]//Fe(100)[010] epitaxial relationship are representative of the whole nanoparticle (see Fig.1).

Five small molecules (H, CO, H_2O, HCOOH and CH_3S^-) were deposited on the following surfaces:

- the Au(001) surface, made of 8 planes,
- the Au(001) surface, made of 8 planes and strained at the lattice parameter of Fe in the xy-plane, named herafter "s-Au(001)",
- the Au(001)/Fe(001) system, with different numbers of Au(001) monolayers (MLs) deposited on 6 Fe(001) planes, named hereafter "Au-nML/Fe" where n is the number of Au(001) monolayers.

The parameters of the surfaces and of the periodic supercells have been carefully chosen in order to avoid finite size effects and

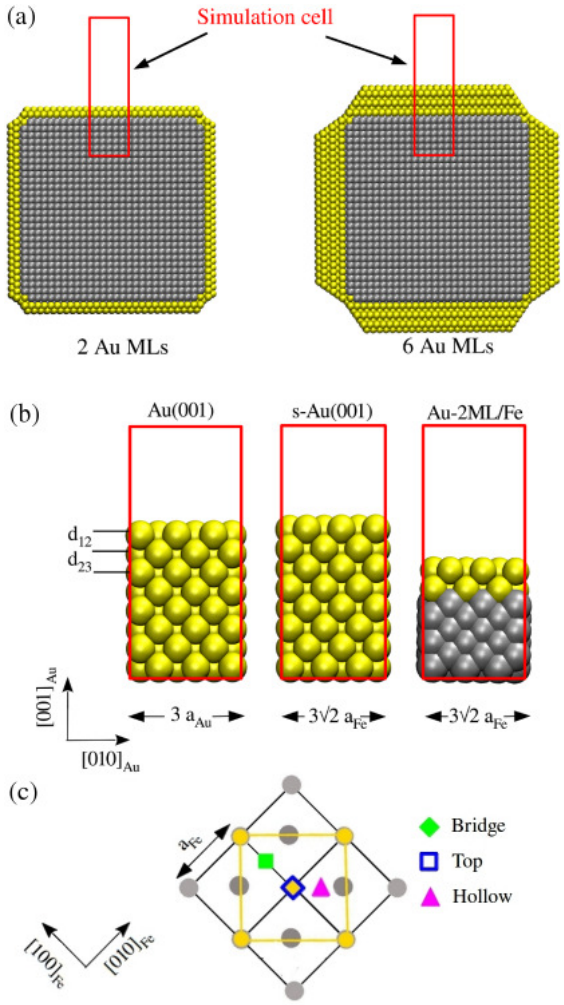

Fig. 1 (a) Schematic representation of the Fe@Au nanoparticles with two different shell thicknesses: 2 Au monolayers (left) and 6 Au monolayers (right). The red rectangles shows the simulation cell of the model systems. (b) Schematic representation of the slabs and the periodic supercells for the three types of studied surfaces. (c) Epitaxial relationship at 45 ° of Au(001) on Fe(001) and adsorption sites. Yellow and grey circles denote Au and Fe atoms, respectively.

to minimize the computational cost. For the size of the supercell in the xy plane, the adsorption energy of the largest molecule, HCOOH, has been used as a probe on the Au(001) surface. The adsorption energy is evaluated as follows:

$$E_{ads} = E(\text{mol/surf}) - E(\text{mol}) - E(\text{surf}) \quad (1)$$

where $E(\text{mol/surf})$ is the total energy of the molecule on the metallic surface, $E(\text{mol})$ is the total energy of the free molecule, and $E(\text{surf})$ is the total energy of the metallic surface, computed in the same conditions.

Convergency of this energy was achieved for a 3x3 cell in the xy plane, indicating that the molecule does not interact with its periodic images beyond this cell size.

Concerning the number of planes to be considered, we examined separately the effect of varying the number of Au planes for the Au(001) surface and the number of Fe(001) planes for the

Au-*n*ML/Fe systems. The variation of E_{ads} for the CO molecule was used in that case. In Fig. 2(a), the adsorption energy of CO adsorbed on Au(001) is shown and in Fig.2(b), this energy when CO is adsorbed on Au-1ML/Fe. Convergency is reached at 8 Au planes for the Au(001) surface and at 6 Fe planes for the Au-1ML/Fe surface.

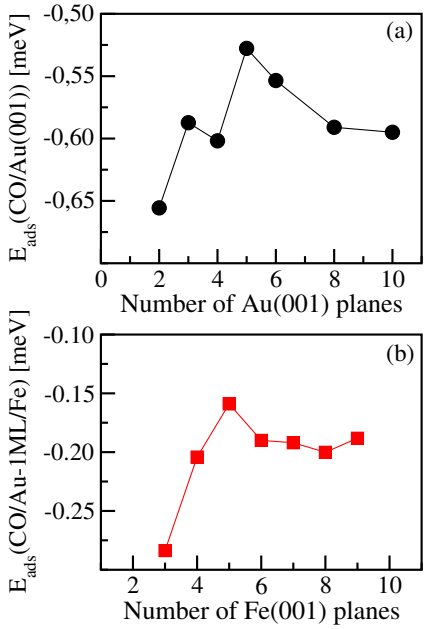

Fig. 2 Variation of the adsorption energy of CO on (a) Au(001) as a function of the number of Au planes in the z direction and (b) on Au-1ML/Fe as a function of the number of Fe planes in the z direction. Calculations have been performed with an energy cutoff of only 400 eV in order to save computing time.

For the following, we thus chose to duplicate the cell 3 times in the x and y direction. For adsorption on Au(001) and s-Au(001), 8 planes were used for the slabs and for the Au(001)/Fe(001) systems, we chose systems with n Au(001) monolayers (n =1,2,3 or 6) deposited on 6 Fe(001) planes. In all cases, the initial atomic positions were extracted from bigger systems that were relaxed for a previous study (see Ref.[36]). The atoms of the two bottom layers were kept fixed to their relaxed positions in the bigger systems. A vacuum of at least 16 Å was introduced in the z direction to separate the slabs from their images.

For the CO molecule, the adsorption on the 6 following systems was studied: Au(001), s-Au(001), Au-1ML/Fe, Au-2ML/Fe, Au-3ML/Fe and Au-6ML/Fe. For the other molecules, only 3 systems were studied: Au(001), s-Au(001) and Au-2ML/Fe. In all cases, only the most stable adsorption site was chosen[9,52,53,58,59].

Calculations have been performed using the DFT package VASP[41], with PAW pseudopotentials and the Perdew-Burke-Ernzerhof (PBE) generalized gradient approximation (GGA) for the exchange and correlation functional, in periodic boundary conditions. For this particular functional, bulk and surface properties have been found in very good agreement with experimental data for iron and in poorer agreement for gold. The corresponding errors have been evaluated in Ref.[36].

For adsorption of molecules on metallic systems, it is well-known that common GGA functionals do not perform very well and that dispersion interactions should be properly accounted for[42]. Beyond the empirical method proposed by S. Grimme[44], there exist currently several modified functionals capable of giving correct adsorption energies of molecules on metallic surfaces[43,45–48]. However, these functionals induce modifications of the bulk properties (lattice parameters, bulk modulus, cohesive energy etc.) and of the surface properties. In the case of gold, these modifications tend to slightly improve the comparison of the computed metal characteristics with experiments[49], whereas degrading the quality of the iron description. The main aim of this work being the study of the ligand effect between gold and iron, we have decided to use the PBE functional, knowing that adsorption energies might be too low compared to experimental values and assuming that dispersion energies are of similar magnitude for all studied cases (all modeled systems present a more or less constrained Au(001) surface).

In all cases, a grid of 4x4x1 special k-points in the Monkhorst-Pack scheme was sufficient to ensure the good convergency of the total energy. A plane-wave cutoff energy of 800 eV was necessary in order to obtain the convergency of the total energy when C atoms were present and, for consistency reasons, we used this energy cutoff for all calculations. A broadening, using the Methfessel and Paxton scheme of order 1, was used with a smearing of 0.05 eV for the electron occupation[50]. For each system, the atomic positions were relaxed until the forces reached a minimum of 10^{-3} eV/Å .

3 Results and discussion

In this section, we present the results regarding the adsorption of several molecules on the different systems described in the Sec. 2. In the first part, we analyze the effect of the strain and of the number of Au MLs epitaxied on the Fe substrate on the adsorption properties of CO, and an explanation of these effects is presented. In the second part, the adsorption properties of the other studied molecules are presented on the system made of 2 Au(001) MLs deposited on Fe(001) and compared to the adsorption on Au(001) and s-Au(001).

3.1 Effect of the number of Au layers on the adsorption of CO

In order to better understand the effect of the Fe substrate, we analyzed the adsorption properties of CO on systems for which the number of Au MLs deposited on Fe(001) has been varied from 1 ML to 6 MLs and compared them to adsorption on Au(001) and strained Au(001).

The CO molecule is chemisorbed in the "bridge" position for all systems. In Figure 3, the positions of the adsorbed CO molecule on the different systems are presented and the values of the main distances are reported. The CO adsorption is accompanied by a slight displacement of the bonded gold atoms (Au_1) above the surface plane and an increase of the Au_1-Au_1 distance in the plane. Indeed, in the surface without the CO molecule, the Au_1-Au_1 distance is given by $\sqrt{2}a_{Au}/2$ which is equal to 2.95 Å for Au(001) and to 2.83 Å for s-Au(001) and for the Au/Fe systems.

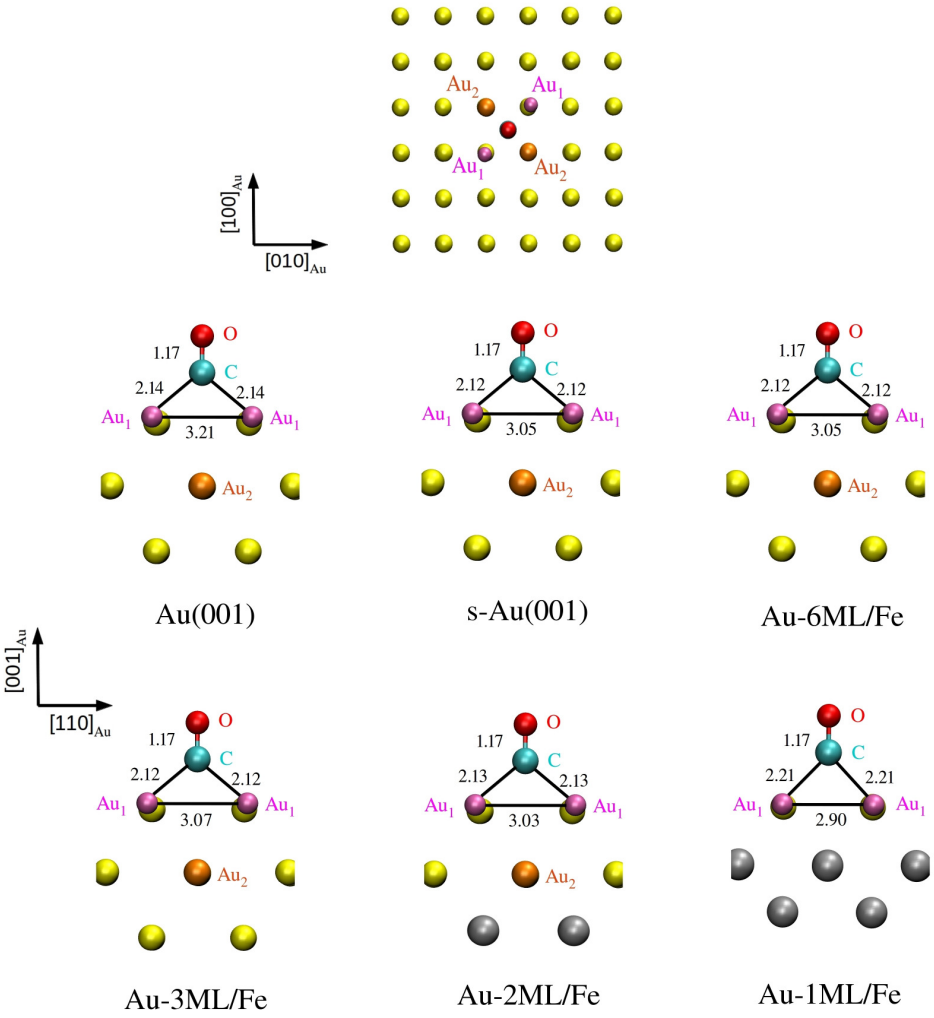

Fig. 3 Top view of the CO molecule adsorbed on the Au(001) surface and side views of the CO molecule adsorbed on the different studied systems: Au(001), strained Au(001) at the Fe lattice parameter (s-Au(001)), and systems made of 1, 2, 3 and 6 Au(001) MLs epitaxied on Fe(001). Atomic distances are reported in Å . The Au_1 atoms (pink circles) are surface atoms bonded to the C atom, the Au_2 atoms (orange) belong to the subsurface and are the next nearest neighbours of the C atom. The other color codes are C: cyan, O: red, Au: yellow, Fe: grey.

These results are in agreement with previous theoretical calculations of the CO adsorption on the Au(001) surface, which found that the bridge site was the most favourable [9,52,53].

3.1.1 Adsorption energy

The variation of the adsorption energy of CO as a function of the number of Au(001) MLs deposited on Fe(001) is shown in Fig.4 and compared to the ones of CO on Au(001) (bold line) and on strained Au(001) (dashed line) surfaces (see also Tab. 1). For Au(001), the adsorption energy of CO is equal to -587 meV, a value which is in good agreement with the experimental value of -602 meV [54] and with previous DFT calculations using the PBE or PW91 functional [52,53]. Note that a much higher adsorption energy (-250 meV) was obtained using the RPBE functional [9].

When the molecule is adsorbed on the strained Au(001) surface, adsorption is weaker than on the unstrained Au(001) surface. Here, the strain due to the lattice mismatch between the bulk parameters of Au and Fe in the PBE approximation is equal to $\varepsilon_{\parallel} = (a_{\mathrm{Fe}} - a_{\mathrm{Au}})/a_{\mathrm{Au}}$ = -3.95 %, i.e. the Au(001) surface is in compression in the xy plane. As will be discussed afterwards, this increase of the adsorption energy could be explained by the fact that the d band is shifted to lower energies in the case of the strained Au(001) surface with respect to that of the Au(001) surface, which makes the strained surface less reactive.

Table 1 Adsorption energies of CO on the different surfaces in meV.

	E_{ads} [meV]	ΔE_{ads} [meV]
Au(001)	-587	0
s-Au(001)	-500	+87
Au-6ML/Fe	-514	+73
Au-3ML/Fe	-499	+88
Au-2ML/Fe	-414	+173
Au-1ML/Fe	-231	+356

The effect of the Fe substrate on the adsorption energy of CO is modulated by the number of epitaxied Au MLs. For 3 and 6 Au MLs, the adsorption energy is comparable to the one on the

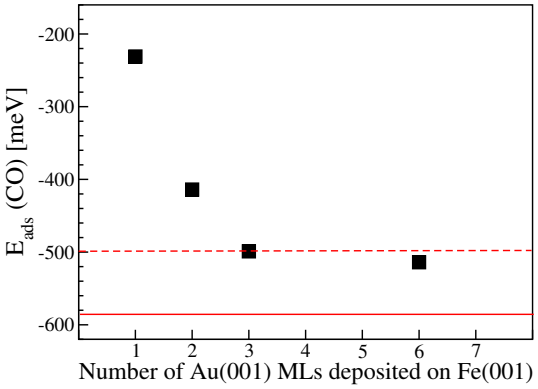

Fig. 4 Evolution of the adsorption energy of CO as a function of the number of Au(001) MLs deposited on Fe(001). The bold (resp. dashed) line corresponds to the adsorption energy obtained when CO is adsorbed on the Au(001) (resp. strained Au(001)) surface.

strained Au(001) surface, i.e. the Fe substrate produces no significant effect appart from the induced compressive lateral strain. However, the situation becomes substantially different when 2 Au MLs are epitaxied on the Fe substrate. In that case, the CO adsorption energy is equal to **-414 meV**, i.e. greater than the adsorption on Au(001) by **+173 meV** and than the adsorption on s-Au(001) by **+86 meV**. This result indicates that, for 2 Au MLs, the effect of the Fe susbtrate is not only a strain effect, but that electronic effects come into play which induce an increase of the adsorption energy. In the case of 1 Au(001) ML eptiaxied on Fe, the situation is quite different since the Fe(001) surface is not entirely covered by gold atoms and the adsorption energy is even greater in that case ($\Delta E = +356$ meV) than for 2 Au MLs. Clearly, for 1 and 2 Au MLs, in addition to the effect of strain due to epitaxy, the molecule 'feels' the presence of the iron substrate, which is characteristic of the ligand effect.

3.1.2 *d*-band states

The strain effect as well as the ligand effect are generally explained by a shift of the *d*-band of the transition metal surface atoms, which induces a change in the surface reactivity[11,20,21]. This effect has been well documented and is present for most of the transition metal surfaces subject to lateral strain[11–16]. A model explaining this effect, named *d*-band model, has been proposed by the Norskov's group in the 90's[18,19]. In this latter, the difference of reactivity when the *d*-band is shifted is explained by a change in the filling of the antibonding state issued from the hybridization between the valence state of the molecule and *d* states of the metal. In a metal, this filling is determined by the energy of the antibonding state relative to the Fermi level. The antibonding state being always above the *d* states, the energy of the *d*-band center relative to the Fermi level is a good first indicator of the bond strength. The higher the *d* states (relative to the Fermi level), the stronger the bond[17–19].

For the Au(001) surface, a compressive in-plane strain should induce a shift of the *d*-band states towards lower values and consequently a lower reactivity. This is indeed what we observe for the adsorption energy of CO which increases when the Au(001) surface is subject to a compressive strain. For the ligand effect, however, the existence of this shift is not straighhtforward since it depends on the two metals put together. In Figure 5, the densities of states projected on the Au surface atoms *d* states (PDOS) are presented for all the studied systems, without the CO molecule. The modification of the *d*-band due to the strain effect is hardly visible on the PDOS. Up to the Au-2ML/Fe system, the PDOS on the Au surface atoms does not seem very different than for Au(001). Only the PDOS obtained for the Au-1ML/Fe system is clearly modified and shifted towards lower energies.

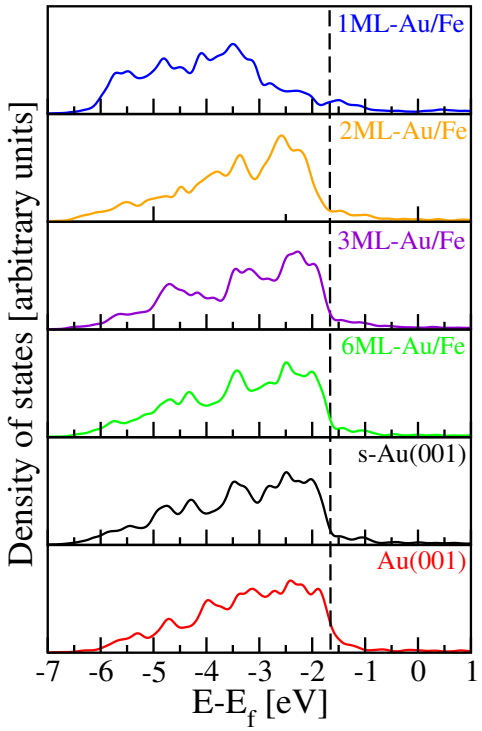

Fig. 5 Densities of states projected on the Au surface atoms *d* states for all the studied systems without the CO molecule. The Fermi level has been put to zero. The vertical dashed line was placed at the upper limit of the *d*-band in the Au(001) system.

It is possible to unravel shifts of the PDOS by calculating the center of the *d*-band ε_d for the Au surface atoms and for the Au subsurface atoms (named hereafter "surf-1") for all the studied systems, without the CO molecule. The average ε_d is obtained by averaging the following quantity over all the surface (or subsurface) atoms:

$$\varepsilon_d = \frac{\int E N_d(E) dE}{\int N_d(E) dE} - E_{\text{fermi}} \qquad (2)$$

where $N_d(E)$ represents the density of states projected onto the surface or subsurface metal atom *d*-band and E_{fermi} is the Fermi level of the system.

In Table 2, the computed values for the *d*-band centers ε_d are given for the surface and subsurface atoms, for all the studied systems. By looking at the difference between ε_d for Au(001) and s-Au(001), one can see that the strain induces a slight shift of the surface *d*-band downwards. Since the increase of the CO adsorption energy due to the strain is quite small (+87 meV), this very small change in the *d*-band could be sufficient to explain it.

Table 2 Values of the average d-band centers ε_d for the surface and subsurface atoms of all the studied systems.

	$\varepsilon_d(\mathrm{Au_{surf}})$ [eV]	$\varepsilon_d(\mathrm{Au_{surf-1}})$ [eV]
Au(001)	-3.20	-3.66
s-Au(001)	-3.36	-3.82
Au-6ML/Fe	-3.34	-3.80
Au-3ML/Fe	-3.29	-3.76
Au-2ML/Fe	-3.36	-4.28
Au-1ML/Fe	-3.93	-

For 6 Au MLs and 3 MLs epitaxied on Fe, the ligand effect is very weak. The corresponding changes in the d-band center for the surface atoms are not very important and can be related to very small changes in the CO adsorption energy. For the 2 Au-2ML/Fe system, despite a larger variation of the adsorption energy, the value of the d-band center is similar to that obtained for 6 and 3 Au-MLs. However, we observe a very different value for the d-band center of the subsurface atoms. Finally, the largest shift of ε_d is obtained for the Au-1ML/Fe system.

A downward shift of the d-band is commonly associated with a lower reactivity. In the particular case of the Au-2ML/Fe system, the lower adsorption energy is not accompanied by a decrease of the d-band center, ε_d. This comes from the fact that ε_d is an average quantity that is not capable to capture slight modifications of the d-band. Indeed, when looking at the upper limit of the d-bands in the different investigated systems, one can observe a slight shift downward as the number of Au MLs is decreased (vertical dashed line in Fig. 5). The ligand effect therefore induces a shift of the upper limit of the d-band towards lower energies and consequently a lower reactivity, as observed for the CO adsorption.

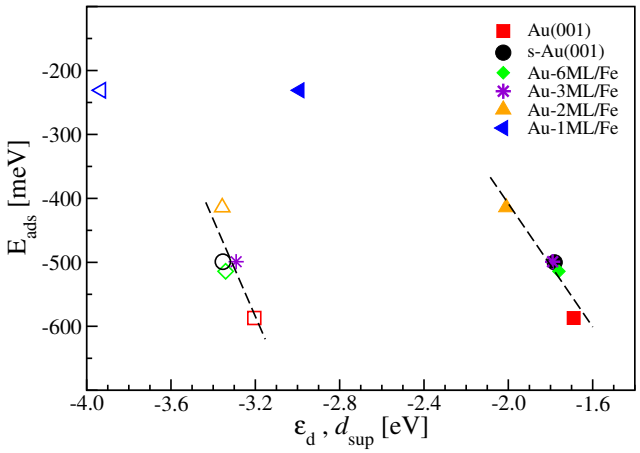

Fig. 6 CO adsorption energy as a function of the average d-band center, ε_d (empty symbols), and as a function of the upper limit of the d-band, d_{sup} (filled symbols), of the Au surface atoms (for clean surfaces) for all the studied systems. The dashed lines correspond to linear fits of the points without the Au-1ML/Fe ones.

The upper limit of the d-band can be approximately computed by simply taking, among the values at half of its height, the one of highest energy, d_{sup}. In Figure 6, $\mathrm{E_{ads}}$ is plotted as a function of ε_d and d_{sup} for the Au surface atoms for all the studied systems. Clearly, the increase of $\mathrm{E_{ads}}$ due to the strain or to the ligand effects is correlated with a shift of the d-band towards lower energy, and in particular of its upper limit. In the literature, a linear correlation between the adsorption energy of a molecule and the shift of the surface atoms d-band center is often obtained [12,14,21,22,33]. In this particular case, the linear correlation between the CO adsorption energy and ε_d or d_{sup} can be obtained for all systems, except the Au-1ML/Fe one. In this latter case, in which the sparse Au(001) monolayer is epitaxied on a metallic substrate, it could be hypothesized that the substrate induces a ligand effect more complex than just a d-band shift. Discrepancies with the d-band model have already been evidenced for the CO adsorption on Pd/Au(111) and Pd/Au(001) [55], and on Pt/Au(001) [53], but also for the adsorption of H and O_2 on strained Cu surfaces [56] and of C, N and O on Pd/X alloys [57].

3.1.3 Distances and charges

To go further in the comprehension of the CO adsorption on these systems, we analyzed in details their main characteristics. In Tab.3, distances between the C and the closest Au atoms belonging to the surface ($\mathrm{Au_1}$) and to the subsurface ($\mathrm{Au_2}$) are given in the first two columns. In the third column, the *average* distance between C and the Au surface is shown, computed as:

$$\delta z(\mathrm{C-surf}) = z(\mathrm{C}) - \frac{1}{N_s}\sum_{i=1}^{N_s} z(\mathrm{Au}_i) \qquad (3)$$

where N_s is the number of Au surface atoms in our systems, $z(C)$ is the z-coordinate of the C atom and $z(Au_i)$ are the z-coordinates of the Au surface atoms. It is followed by the distance between C and the $\mathrm{Au_1}$ atoms projected on the direction perpendicular to the surface ($\delta z(\mathrm{C\text{-}Au_1})$) and by the distance between the $\mathrm{Au_1}$ atoms and the surface, computed as:

$$\delta z(\mathrm{Au_1-surf}) = z(\mathrm{Au_1}) - \frac{1}{N_s-2}\sum_{i=1,i\neq \mathrm{Au_1}}^{N_s} z(\mathrm{Au}_i). \qquad (4)$$

The next two columns present the interplanar distance, $\mathrm{d_{12}}$ and $\mathrm{d_{23}}$, where the index 1, 2 and 3 denote the surface, the subsurface and the subsubsurface, respectively. The Bader charges on the $\mathrm{Au_1}$ atoms are given in the last column.

The strain state of the s-Au(001) surface results in a decrease of the C-$\mathrm{Au_1}$ bond lengths from 2.138 Å to 2.125 Å. Except for the Au-1ML/Fe system, the C-$\mathrm{Au_1}$ distances are within these two values. In the Au-1ML/Fe system, the C-$\mathrm{Au_1}$ bond lengths are much longer (2.206 Å), the Au(001) surface is less modified and the adsorption energy is much weaker. These differences in adsorption distances and modification of the surface do not affect the CO intra-molecular distance which is equal to 1.17 Å in all systems.

The longer C-$\mathrm{Au_1}$ distance in the Au-1ML/Fe system is accompanied by a higher charge on the $\mathrm{Au_1}$ atom of 11.22 e compared to the charge of 11 e for the bulk Au atom in our DFT calculations). However it is quite intringing that, for the case of 2 Au MLs, the increase of the adsorption energy is not correlated with a C-$\mathrm{Au_1}$ bond length increase. In this particular case, the C-$\mathrm{Au_1}$ distance is similar than for all the other Au/Fe systems, while the C-$\mathrm{Au_2}$ distance is increased due to the presence of the iron sub-

Table 3 Distances between C and the first neighbouring surface Au atoms (Au_1) and the second neighbouring subsurface Au atoms (Au_2), difference between the z-coordinate of the C atom and the average z-coordinate of the Au surface atoms (δz(C-surf)), difference between the z-coordinates of the C atom and the Au_1 atoms (δz(C-Au_1)), difference between the z-coordinate of the Au_1 atoms and the average z-coordinate of the Au surface atoms (δz(Au_1-surf)), interplanar distances between the three Au (or Fe) top layers (d_{12} and d_{23}), Bader charges of the Au_1 atoms (see Figure 3).

	d(C-Au_1) [Å]	d(C-Au_2) [Å]	δz(C-surf) [Å]	δz(C-Au_1) [Å]	δz(Au_1-surf) [Å]	d_{12} [Å]	d_{23} [Å]	q(Au_1) [e]
Au(001)	2.138	3.906	1.561	1.409	0.171	2.058	2.088	10.94
s-Au(001)	2.125	4.117	1.662	1.481	0.204	2.212	2.224	10.93
Au-6ML/Fe	2.122	4.107	1.655	1.476	0.203	2.211	2.216	10.93
Au-3ML/Fe	2.119	4.094	1.632	1.463	0.190	2.227	2.246	10.93
Au-2ML/Fe	2.127	4.175	1.622	1.495	0.135	2.243	1.857(Fe)	10.95
Au-1ML/Fe	2.206	3.889(Fe)	1.716	1.665	0.058	1.874(Fe)	1.475(Fe)	11.22

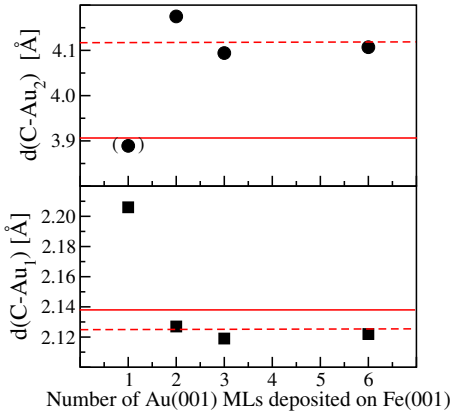

Fig. 7 Evolution of the C-Au_1 (bottom) and C-Au_2 (top) distances as a function of the number of Au layers epitaxied on Fe(001) and compared to the values for Au(001) (bold line) and strained Au(001) (dashed line). The circle in parenthesis corresponds to a C-Fe distance.

strate. These results are depicted in Figure 7 where the C-Au_1 and C-Au_2 distances are plotted as a function of the number of Au layers and compared to the values obtained for Au(001) (bold line) and s-Au(001) (dashed line).

Let us now compare the CO molecule adsorbed on the strained Au(001) surface and on the Au-2ML/Fe one, which will allow to discriminate the ligand effect from the strain effect. In the case of s-Au(001), the C-Au_1 distance is equal to 2.125 Å , the Au_1-Au_1 distance to 3.048 Å and the Au_1 atoms are displaced above the surface by δz(Au_1-surf) +0.204 Å . Comparatively, in the Au-2ML/Fe system, the C-Au_1 distance is equal to 2.127 Å , the Au_1-Au_1 distance to 3.026 Å and the Au_1 atoms are displaced above the surface by δz(Au_1-surf) +0.135 Å. This smaller shift of the Au_1 atoms above the surface is accompanied by a slightly larger charge on the Au_1 atoms (10.95 e). Overall, in the case of the Au-2ML/Fe system, the bond distances are not very different than in the case of s-Au(001), but the CO molecule is further away from the Au_1 atoms in the direction perpendicular to the surface.

The Au_1 atoms move away from the surface due to their bonding with the carbon atom of the CO molecule. However, the fewer the number of Au MLs, the less the Au_1 atoms move away from the surface. For Au-1ML/Fe and Au-2ML/Fe, this is due to a strong coupling between the Fe substrate and the Au surface layers[36] which prevents the Au_1 to go out from the Au surface.

The analysis of the geometry and charges indicates that the CO adsorption energy might be correlated with the distance between the CO molecule and the Au_1 atoms, projected on the direction perpendicular to the surface (δz(C-Au_1)). A correlation is indeed obtained between the C-Au_1 distance perpendicular to the surface and the adsorption energy E_{ads} as shown in Figure 8, where the variation of this distance with respect to the Au(001) one is plotted as a function of the variation of E_{ads} with respect to the Au(001) one (ΔE_{ads}, see Tab. 1). The correlation is linear with a correlation coefficient R=0.977.

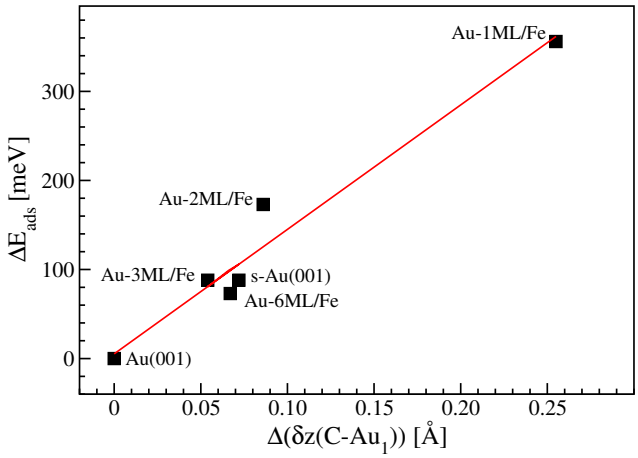

Fig. 8 Variation of the CO adsorption energy as a function of the variation of the distance between C and the Au_1 atoms (δz(C-Au_1)), in the direction perpendicular to the surface, with respect to the values obtained for Au(001), for all the studied systems.

3.1.4 Potential energy curve

In order to understand the origin of this effect, we rigidly moved the CO molecule from the previously relaxed surface and computed the corresponding interaction energy E_{int} without relaxing the geometry for the new positions:

$$E_{int} = E^{ur}(mol/surf) - E^{ur}(mol) - E^{ur}(surf) \quad (5)$$

where *ur* stands for "unrelaxed". The results are presented in Figure 9, where the values of E_{int} are plotted as a function of δz (C-Au_1), for all the studied systems (note that E_{int} is different from E_{ads} since it does not take into account the relaxations).

Two major information can be drawn from these curves. First the minima are actually shifted towards larger distances and higher energies when the substrate is strained (Au(001) → s-Au(001)) and when the ligand effect comes into play (s-Au(001) → Au-2ML/Fe and Au-1ML/Fe). The minima for Au-6ML/Fe and

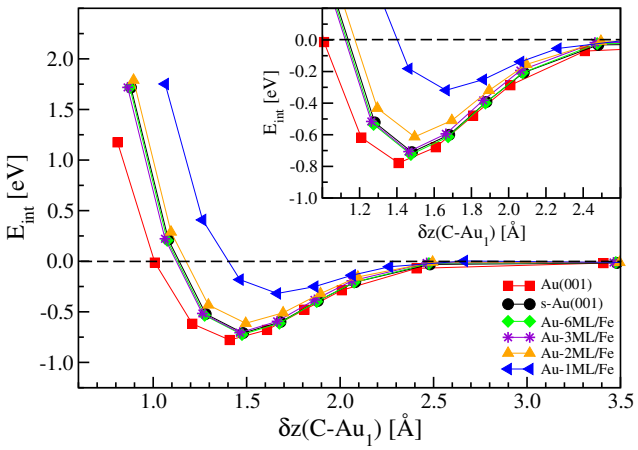

Fig. 9 Interaction energy E_{int} computed by rigidly moving the CO molecule from the surface, as a function of the distance between C and the surface atoms, for all the studied systems. Inset: zoom on the minima region.

Au-3ML/Fe are superimposed with the s-Au(001) one. Second, we observe that the repulsive part of the curve is strongly modified when the Au(001) surface is subject to strain and to the ligand effect. This change of the minimum position and of the repulsion part of the potential energy surface can indeed explain the change in the CO adsorption energy observed in the studied systems.

To summarize, the CO adsorption energy is increased due to the strain induced by the epitaxy of Au(001) on Fe(001) for more than 2 Au MLs, and due the strain *and* ligand effects for 1 and 2 Au MLs. The variation of E_{ads} is induced by a shift of the *d*-band states of the surface atoms towards lower energy. Besides, a linear correlation was found between the CO adsorption energy and the distance between the C atom and the surface, which is influenced by the distance to the subsurface layer and its nature, as they change the repulsive part of the potential energy surface.

3.2 Adsorption of small molecules on 2 Au MLs epitaxied on Fe(001)

From the study of the CO adsorption on the Au/Fe systems, we have found that the strongest increase of the adsorption energy is obtained for 1 Au(001) ML epitaxied on Fe(001). However, at this coverage, the Fe surface is not totally protected by gold and might still be accessible to oxidation. Besides, the strain and ligand effects are still quite significant for CO adsorbed on 2 Au(001) ML epitaxied on Fe(001). We therefore decided to study these effects on this latter system for other small molecules following the protocol established for the adsorption of CO on the different surfaces.

In order to discriminate between the two effects (strain and ligand), we computed the adsorption on three different systems: Au(001), s-Au(001) and Au-2ML/Fe. The chosen molecules (or atoms) are H, H_2O, HCOOH and CH_3S^- which were selected for their representativity in the types of bonding with metallic surfaces. Figure 10 shows the adsorption geometries of these molecules on the different surfaces. Top views are presented on the left and the three other columns present the corresponding side views with the main atomic distances for the three studied surfaces. The positions of the adsorbed molecules correspond to the most stable positions on Au(001) [53,58,59].

The main characteristics of the systems are given in Table 4: distance between the bonding atoms of the molecules and the surface atoms (d(X-Au)), projection of this distance on the direction perpendicular to the surface (δz(X-surf)), and charge variation of the molecule after adsorption (Δq(mol)). The CO, H and CH_3S^- molecules are chemisorbed and the H_2O and HCOOH are physisorbed. One can note that, for the chemisorbed molecules, the trends are similar than for CO. Namely, the bond lengths between the molecule and the Au atoms of the surface do not change much due to the strain and/or the ligand effect, whereas, for H_2O and HCOOH, the distance between the molecule and the Au atoms increases.

Table 4 Distance between the molecule and the closest Au surface atoms d(X-Au), projection of this distance on the direction perpendicular to the surface δz(X-Au) and modification of the molecular charge Δq(mol), for the three surfaces. X denotes the atom of the molecule which is closest to the surface.

	H bridge	CO bridge	CH_3S^- hollow	H_2O top	HCOOH -
d(X-Au) [Å]					
Au(001)	1.775	2.138	2.416	2.678	2.628(O) 2.476(H)
s-Au(001)	1.772	2.125	2.429	2.757	2.736(O) 2.500(H)
Au-2ML/Fe	1.767	2.127	2.434	2.817	2.779(O) 2.503(H)
δz(X-Au) [Å]					
Au(001)	0.907	1.409	1.683	2.661	2.595(O) 2.274(H)
s-Au(001)	1.002	1.481	1.815	2.743	2.701(O) 2.326(H)
Au-2ML/Fe	0.990	1.495	1.820	2.804	2.755(O) 2.346(H)
Δq(mol) [*e*]					
Au(001)	+0.04	+0.10	+0.03	-0.05	-0.02
s-Au(001)	+0.04	+0.09	+0.03	-0.05	-0.02
Au-2ML/Fe	+0.03	+0.10	+0.04	-0.04	-0.01

The corresponding adsorption energies of these molecules on the three different surfaces are given in Table 5 in which the contributions from the strain and ligand effects have been separated: $\Delta E_{ads}(strain)$ = E_{ads}(s-Au(001))-E_{ads}(Au(001)), $\Delta E_{ads}(ligand)$ = E_{ads}(Au-2ML/Fe) - E_{ads}(s-Au(001)), and $\Delta E_{ads}(total)$= E_{ads}(Au-2ML/Fe) - E_{ads}(Au(001)). On the Au(001) surface, they are in agreement with the adsorption energies computed using DFT found in the literature [53,58–60]. Evidently, for H_2O and even for HCOOH, the lack of dispersion interactions leads to too high adsorption energies compared to experiments. However, since we wish to evaluate the effect of strain and of the substrate on the adsorption energies and structures of molecules deposited on the same surface, i.e. Au(001), in a first approximation, we will assume that the dispersion is equivalent for the three different surfaces.

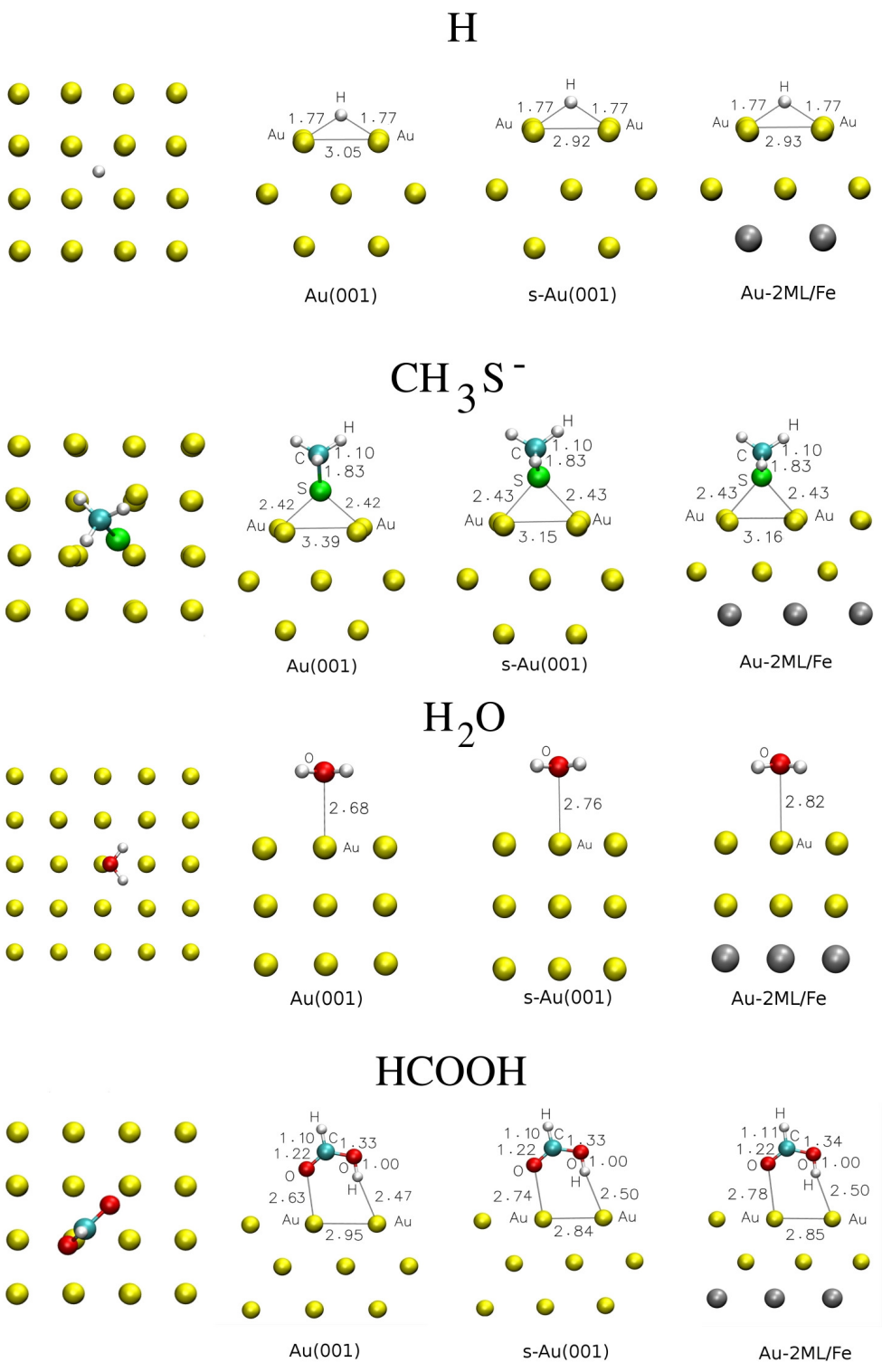

Fig. 10 Left: top views of the adsorption of the different molecules on the Au(001) surface. The other three columns correspond to the side views of the adsorption of the molecules on Au(001), strained Au(001) and Au-2ML/Fe systems. C: cyan, O: red, Au: yellow, Fe: gray, H: white, S: green.

In order to check this, we computed the van der Waals energy between the H_2O molecule and the Au surface (at fixed geometry) using the Grimme's potential[44] and found that it is equal to -70 meV for Au(001) and -72 meV for Au-2ML/Fe. This result indicates that the dispersion interactions are of the same order for the different studied surfaces and that neglecting them does not affect the reasoning.

Table 5 Adsorption energies, E_{ads} in meV, for the different studied molecules in their most stable configurations. Three surfaces are considered: Au(001), s-Au(001) and Au-2ML/Fe. $\Delta E_{ads}(strain)$ = E_{ads}(s-Au(001))-E_{ads}(Au(001)), $\Delta E_{ads}(ligand)$ = E_{ads}(Au-2ML/Fe) - E_{ads}(s-Au(001)), and $\Delta E_{ads}(total)$= E_{ads}(Au-2ML/Fe) - E_{ads}(Au(001)).

	H bridge	CO bridge	CH_3S^- hollow	H_2O top	HCOOH -
Au(001) E_{ads}	-2243	-587	-2216	-149	-177
s-Au(001) E_{ads}	-2178	-500	-2012	-126	-148
Au-2ML/Fe E_{ads}	-2147	-414	-1930	-116	-149
$\Delta E_{ads}(strain)$	+65	+87	+204	+23	+29
$\Delta E_{ads}(ligand)$	+31	+86	+82	+10	-1
$\Delta E_{ads}(total)$	+96	+173	+286	+33	+28

In the case of strained Au(001), the in-plane compression leads to the increase of the adsorption energy for all molecules, but with different magnitudes. The largest increase is obtained for CH_3S^- for which the adsorption energy increases by +204 meV, whereas for H_2O, the adsorption energy increases by only +23 meV. Concerning the ligand effect solely, the most important increase of the adsorption energy due to the presence of the Fe substrate is obtained for CO then for CH_3S^- and then for H. The other molecules, H_2O and HCOOH, are less, or even not at all, sensitive to this effect. More generally, for the two physisorbed molecules, the adsorption seems to be less affected by a change of the surface properties, whether it is a strain or a ligand effect. However, even if the adsorption energy is not much different, their distance to the Au surface atoms increases significantly.

In the case of CO, the strain and ligand effects induce a modification of the potential energy surface seen by the molecule as it approaches the surface. It is interesting to see whether the same modification occurs for the other chemisorbed molecules, i.e. H and CH_3S^-. For all molecules, except H, the strain and ligand effects induce an increase of the distance between the molecules and the Au atoms δz(X-Au) which is correlated with the increase of the adsorption energy. In Figure 11(a), the variations of adsorption energies are plotted as a function of the molecule-surface distances with respect to the values obtained for Au(001), for all the studied molecules. In Figures 11(b) and (c), the variation of the adsorption energies due solely to the strain effect and solely to the ligand effect are shown, respectively.

In the case of H_2O (red squares) and HCOOH (blue triangles), which are physisorbed, the situation is very similar: the adsorption energy increases slightly while the molecules move away from the surface and this effect is equally due to the strain and ligand effects. For CH_3S^-, we observe the strongest effect: The adsorption energy is strongly increased by the strain, but also by

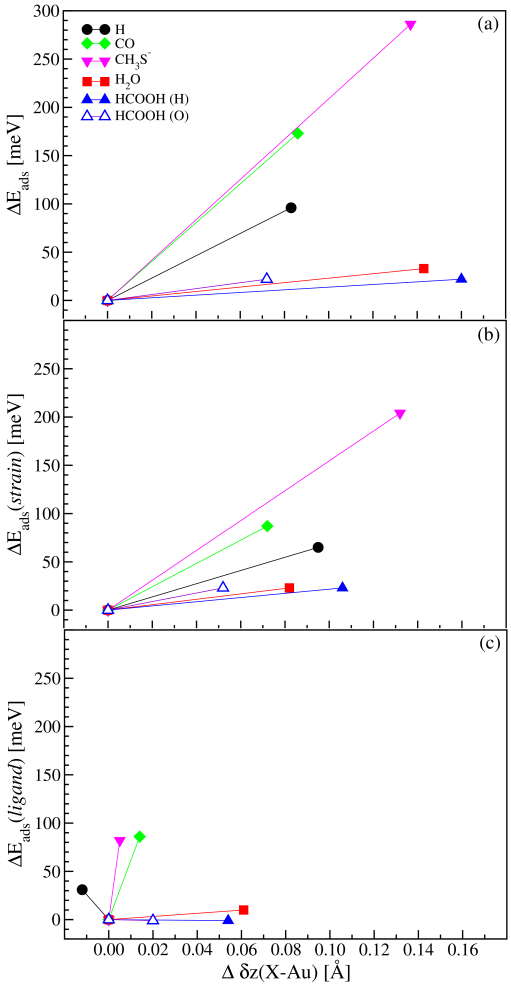

Fig. 11 (a) Variation of the adsorption energy ΔE_{ads} on Au-2ML/Fe as a function of the variation of $\delta z(X-Au)$ with respect to adsorption on Au(001) (see text for definition). (b) Variation of adsorption energy $\Delta E_{ads}(strain)$ due to the strain effect as a function of the variation of $\delta z(X-Au)$ with respect to adsorption on Au(001). (c) Variation of adsorption energy $\Delta E_{ads}(ligand)$ due to the ligand effect as a function of the variation of $\delta z(X-Au)$ with respect to adsorption on s-Au(001).For HCOOH, the two closest atoms (O and H) have been considered.

the presence of the Fe substrate, and the distance between the molecule and the Au surface atoms increases as well. For CO, the behavior is similar than for CH3S$^-$ but the global effect is weaker. Finally, for atomic H, we notice quite a different behavior: The adsorption energy is modifiied by the strain and the H-surface distance is slightly increased. However, for adsorption on Au-2ML/Fe, the adsorption energy increases whereas the distance between H and the surface decreases with respect to that on the s-Au(001) surface. Moreover, the H-Au_1 bond length becomes even slightly smaller (see Tab. 4).

In order to better understand the behavior of adsorbed H on the Au surface, we computed the variation of E_{int} as a function of the distance between H and the surface (Eq.5). The results are presented in Figure 12 for H adsorbed on Au(001), on s-Au(001) and on Au-2ML/Fe. The first thing to notice is that there is a much less repulsive part at small distances, rather an energy barrier

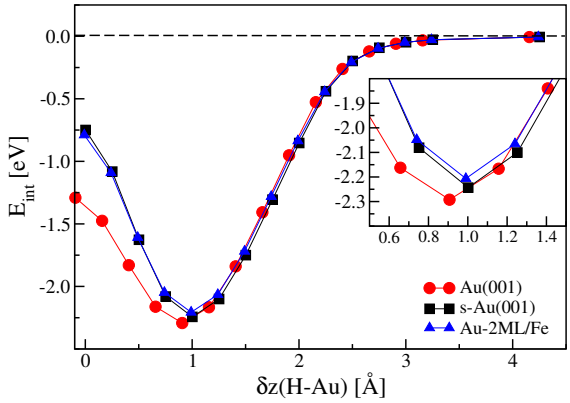

Fig. 12 Interaction energy E_{int} computed by rigidly moving the H atom from the surface, as a function of the distance between H and the surface atoms, for Au(001), s-Au(001) and Au-2ML/Fe. Inset: zoom of the minima region.

of ≈ +0.943 eV for Au(001), +1.509 eV for s-Au(001) and of +1.405 eV for Au-2ML/Fe. This is in agreement with the fact that hydrogen can diffuse inside the metal and is found stable into the subsurface layer[58]. In Ref.[58], the activation energy barrier for the diffusion of H to the subsurface layer is found to be equal to 0.65 eV for Au(001). The discrepancy with our value comes from the fact that we only considered a perpendicular path to the subsurface instead of the minimum energy path and no atomic relaxations.

Regarding the difference between H adsorption on Au(001), s-Au(001) and on Au-2ML/Fe, we observe two different effects. First, when a strain is applied to the Au(001) surface, the distance between the Au atoms in the plane decreases and the H atom undergoes a larger repulsion from the Au(001) surface layer, similarly to what was observed for CO (see Fig. 9). This induces an increase of the barrier height and a small shift of the minimum position away from the surface. When 2 MLs of Au are epitaxied on Fe(001), the effect of the iron subsurface layer comes into play. In this case, the barrier height is slightly lower than for s-Au(001) (≈ -100 meV), the energy minimum is shifted to higher values but the minimum position removes unchanged. One can suppose that the repulsive ligand effect is here compensated by an attraction between the H atom and the subsurface layer. This attractive-repulsive interplay is certainly at the origin of the diffusive properties of H in gold.

4 Conclusion

In this paper, we have computed the variation of the adsorption energy of small molecules on the Au(001) surface when it is epitaxied on a Fe(001) substrate, using DFT. For all the studied molecules, the iron substrate induces a weakening of the binding between the molecule and the surface, which magnitude depends on the type of interaction, chemisorption or physisorption. We have investigated separately the strain effect from the ligand effect and showed that the ligand effect comes into play when only 1 and 2 Au MLs are epitaxied on Fe(001). We have shown that these two effects induce a modification of the repulsive part of the potential energy curve and, for CO, a linear correlation was found between the molecule-surface distance and the adsorption energy. The lower reactivity of the Au surface when it is epitaxied on iron, is due to a shift of the *d*-band of the Au surface atoms towards lower values. As generally admitted, we found that the molecular adsorption energy is linearly correlated with the *d*-band center and with the *d*-band upper limit, except for 1 Au ML. This different behavior for 1 Au ML could be explained by the low compacity of the Au(001) surface.

Fe@Au core-shell nanoparticles are very promising systems for biomedical applications because they gather the magnetic properties of the iron core and the biocompatibility of the gold shell. Here the gold shell prevents the oxidation of the iron core, protects the biological environment from the potential toxicity of the iron and allows the binding of active molecules (most of them bind with gold through a sulfur atom). According to our calculations, it is possible to tune the adsorption energy of small molecules by varying the shell thickness in the recently synthesized Fe@Au nanoparticles[35]. For very thin shells (1 and 2 Au MLs), the adsorption of small molecules can be greatly prevented while keeping the ability of adsorbing thiols. However, since for 1 Au ML coverage the iron core might be accessible to oxidation, 2 Au MLs appear to be the optimum coverage.

Fe@Au core-shell nanoparticules exhibit other crystalline facets than the studied Au(001) one (mainly Au(111)), as well as edges and corners, in which low coordinated Au atoms are present. Studying the effect of the iron substrate on the Au(111) facet and on highly reactive undercoordinated atoms would be necessary in order to draw a global picture of the reactivity of Fe@Au nanoparticles. Work in this direction is in progress.

5 Acknowledgments

Helpful discussions with Dr. Marie-José Casanove, Dr. Hao Tang and Dr. Nicolas Combe are gratefully acknowledged. This work was granted access to the HPC resources of CALMIP under the allocation p1141. The work presented here was supported by a CNRS-Inphyniti Grant (ATHENA 2015 project).

References

1 G.A. Somorjai and Y. Li, *Introduction to Surface Chemistry and Catalysis, 2nd Edition*, (Wiley-Blackwell) (2010).
2 J. M. Thomas and W. J. Thomas, *Principles and Practice of Heterogeneous Catalysis*, (Wiley VCH) (1996).
3 D. Astruc, *Nanoparticles and catalysis*, Ed. by D. Astruc (Wiley-VCH Verlag GmbH & Co. KGaA) (2008).
4 B. Hvolbaek, T.V.W. Janssens, B.S. Clausen, H. Falsig, C.H. Christensen and J.S. Nørskov, Nanotoday **2**, 14 (2007).
5 Z.-P. Liu, Z-Q. Gong, J. Kohanoff, C. Sanchez and P. Hu, Phys. Rev. Lett. **91**, 266102 (2003).
6 M.S. Chen and D.W. Goodman, Science **306**, 252 (2004).
7 M. Chen, Y. Cai, Z. Yan and D.W. Goodman, J. Am. Chem. Soc. **128**, 6341 (2006).
8 A.A. Herzing, C.J. Kiely, A.F Carley, P. Landon and G.J Hutchings, Science **321**, 1331 (2008).
9 G.F. Barmparis and I.N. Remediakis, Phys. Rev. B **86**, 085457 (2012).

10 B. Roldan Cuenya, Accounts of chemical research **46**, 1682 (2013).

11 A. Ruban, B. Hammer, P. Stoltze, H.L. Skriver and J.K. Nørskov, J. Mol. Catal. A: Chem. |bf 115, 421 (1997).

12 M. Mavrikakis, B. Hammer, and J.K. Nørskov, Phys. Rev. Letters **81**, 2819 (1998).

13 M. Mavrikakis, P. Stoltze and J.K. Nørskov, Catal. Letters **64**, 101 (2000).

14 Ph. Sautet, *Stress and Strain in Epitaxy: Theoretical Concepts, Measurements and Applications: Theoretical Concepts, Measurements and Applications*, Ed. J.-P. Deville, M. HanbÃijcken (Elsevier), 155 (2001).

15 A. Logadottir and J.K. Nørskov, Surf. Science **489**, 135 (2001).

16 X. Zhang and G. Lu, J. Phys. Chem. Lett. **5**, 292 (2014).

17 S. Holloway, B.I. Lundqvist, and J.K. NÃÿrskov, Proceedings of the Eighth Conference on Catalysis, Electronic factors in catalysis (Springer, Berlin), IV, p 85 (1984).

18 B. Hammer and J.K. Nørskov, Nature **376**, 2238 (1995).

19 B. Hammer and J.K. Nørskov, Adv. Catal. **45**, 71 (2000).

20 V. Pallassana, M. Neurok, L.B. Hansen, B. Hammer and J.K. Nørskov, Phys. Rev. B **60**, 6146 (1999).

21 A. Schlapka, M. Lischka, A. Groß, U. Käsberger and P. Jakob, Phys. Rev. Lett. **91** 016101 (2003).

22 J.R. Kitchin, J.K. Nørskov, M.A. Barteau and J.G. Chen, J. of Chem. Phys. **120**, 10240 (2004).

23 J. Zhang, M.B. Vukmirovic, Y. Xu, M. Mavrilakis, and R.R. Adzic, Angew. Chem. Int. Ed. **44**, 2132 (2005).

24 A. Groß, Topics in Catalysis **37**, 29 (2006).

25 H.E. Hoster, O.B. Alves, and M.T.M. Koper, ChemPhysChem **11**, 1518 (2010).

26 A.U. Nilekar, A. Alayogu, B. Eichhorn, and M. Mavrikakis, J. Am. Chem. Soc. **132**, 7418 (2010).

27 I.E.L. Stephens *et al.*, J. Am. Chem. Soc. **133**, 5485 (2011).

28 L. Yang *et al.*, J. Phys. Chem. C **117**, 1748 (2013).

29 D. Wang, H. L. Xin, R. Hovden, H. Wang, Y. Yu, D.A. Muller, et al., Nat. Mater. **12**, 81-87 (2013).

30 S. Stolbov and S. Zuluaga, J. Phys. Chem. Lett. **4**, 1537 (2013).

31 S.Jalili, A.Z. Isfahani, and R. Habibpour, International Journal of Industrial Chemistry **4**, 33 (2013).

32 T.A.G. Silva, E. Teixeira-Neto, N. Lopez and L.M. Rossi, Sci. Rep. **4**, 5766 (2014).

33 I.A. Pasti, N.M. Gavrilov and S.V. Mentus, Electrochim. Acta **130**, 453 (2014).

34 S. Goto, S. Hosoi, R. Arai, S. Tanaka, M. Umeda, M. Yoshimoto, and Y. Kudo, J. Phys. Chem. C **118**, 2634 (2014).

35 C. Langlois, P. Benzo, R. Arenal, M. Benoit, J. Nicolai, N. Combe, A. Ponchet, and M. J. Casanove, Nanoletters **15**, 5075 (2015).

36 M. Benoit, C. Langlois, N. Combe, H. Tang and M.-J. Casanove, Phys. Rev. B **86**, 075460 (2012). and Phys. Rev. B **87**, 119905 (2013).

37 M. Benoit, N. Combe, A. Ponchet, J. Morillo, and M.-J. Casanove, Phys. Rev. B **90**, 165437 (2014).

38 D. Huber, Small **1** 482 (2005).

39 S. Kayal, R.R. Vijayaraghavan, J. Nanosci. Nanotechnol. **10** 1 (2010).

40 K. McNamara and S. A. M. Tofail, Phys. Chem. Chem. Phys. DOI 10.1039/C5CP00831J (2015).

41 J. Hafner, Acta Materialia **48**, 71 (2000).

42 A. Tkatchenko, Adv. Func. Mat. 25, 2054-2061 (2015).

43 M. Dion, H. Rydberg, E. SchrÃűder, D. C. Langreth, and B. I. Lundqvist, Phys. Rev. Lett. 92, 246401 (2004).

44 S. Grimme, J. Antony, T. Schwabe, and C. MÃijck-Lichtenfeld, Org. Biomol. Chem. 5, 741 (2007).

45 T. Sato, T. Tsuneda, and K. Hirao, J. Chem. Phys. 126, 234114 (2007).

46 A. Tkatchenko and M. Scheffler, Phys. Rev. Lett. 102, 073005 (2009).

47 J. Klimes, D.R. Bowler, and A. Michaelides, Phys. Rev. B **83**, 195131 (2011).

48 N. Ferri, R.A. DiStasio Jr., A. Ambrosetti, R. Car, and A. Tkatchenko, Phys. Rev. Lett. **114**, 176802 (2015).

49 N. Tarrat, M. Benoit, M. Giraud, A. Ponchet, and M-J. Casanove, Nanoscale **7**, 14515 (2015).

50 M. Methfessel and A.T. Paxton, Phys. Rev. B **40**, 3616 (1989).

51 J.P. Perdew, A. Ruzsinszky, G.I. Csonka, O.A. Vydrov, G.E. Scuseria, L.A. Constantin, X. Zhou, and K. Burke, Phys. Rev. Lett. **100**, 136406 (2008).

52 A. Hussain, D. Curulla Ferré, J. Garcia, B.E. Nieuwenhuys, and J.W. Niemantsverdriet, Surf. Science **603**, 2734 (2009).

53 Y. Yu, X. Wang and K.H. Lim, Catal. Lett. **141** 1872 (2011).

54 R. Meyer, C. Lemire C, S.K. Shaikhutdinov, and H.J. Freund, GOLD BULLETIN **37**. 72 (2004).

55 A. Roudgar and A. Groß, J. Electroanal. Chem. **548**, 121 (2003).

56 S. Sakonga nd A. Groß, Surf. Sci. **525**, 107 (2003).

57 H. Xing, A. Vojdovic, J. Voos„ J.K. Norskov, F. Abild-Pedersen, Phys. Rev. B **89**, 115114 (2014).

58 P. Ferrin, S. Kandoi, A.U. Nilekar, and M. Mavrikakis, Surf. Science **606**, 679 (2012).

59 Z. Jiang, M. Li, T. Yan, and T. Fang, Appl. Surf. Science **315**, 16 (2014).

60 H. Hakkinen, Nature Chemistry 4, 443âĂŞ455 (2012).